DOI: 10.1002/ejoc.200800219

Synthesis, X-ray Crystal Structures, and Solid-State Fluorescence Properties of 5,5-Dialkyl-9-dibutylamino-5*H*-benzo[*b*]naphtho[1,2-*d*]furan-6-one and 3,3-Dialkyl-9-dibutylamino-3*H*-benzo[*kl*]xanthen-2-one[‡]

Yousuke Ooyama,*[a] Akiko Hayashi,[a] Tomohiro Okamoto,[a] Haruka Egawa,[a] Toshiki Mamura,[a] and Katsuhira Yoshida*[a]

Keywords: Crystal structure / Dyes/pigments / Fluorescence / Oxygen heterocycles / Substituent effects

Heterocyclic fluorophores 5,5-dibutyl-9-dibutylamino-5*H*-benzo[*b*]naphtho[1,2-*d*]furan-6-one (**4**) and 3,3-dibutyl-9-dibutylamino-3*H*-benzo[*kl*]xanthen-2-one (**7**) with dialkyl substituents linked in a nonconjugated fashion to the chromophore skeleton have been derived from quinol-type compounds **1** and **2**, and their photophysical properties were investigated in solution and in the solid state. Fluorophores **4** and **7** exhibit strong fluorescence intensity in the solid-state relative to that of quinols **1** and **2**; however, **1** and **4** or **2** and **7** exhibit similar fluorescence intensities in solution. To elucidate the dramatic effect of the dialkyl substituent on the solid-state fluorescence excitation and emission spectra, we performed semiempirical molecular orbital calculations (AM1 and INDO/S) and X-ray crystallographic analysis. On the basis of the results of the calculations and the X-ray crystal structures, the relation between the solid-state photophysical properties and the chemical and crystal structures of **4** and **7** were discussed. It was confirmed that introduction of bulky dialkyl substituents to the fluorophore skeleton can efficiently prevent the short π–π contact between the fluorophores in molecular aggregation states and cause a dramatic solid-state fluorescence enhancement.

Introduction

In recent years, a great concern has been raised about the enhancement of solid-state fluorescence of organic fluorophores, which is the essential subject for the optoelectronic industry for the development of light-emitting diodes[1] and for photoelectric conversion.[2] Much research has been conducted on the correlation between the solid-state fluorescence properties and the molecular packing structures of fluorophores on the basis of their X-ray crystal structures. It has been clarified that strong face-to-face intermolecular π–π interactions between parallel neighboring fluorophores[3–6] or continuous intermolecular hydrogen bonding[4b,7] was a main factor contributing to fluorescence quenching in the solid state. Consequently, the key point in the design of new, strong, solid-state-emissive fluorophores is to remove the intermolecular interactions between fluorophores that cause fluorescence quenching in molecular aggregation states. Yamaguchi et al. recently reported that donor–acceptor–donor-type, solid state strongly fluorescent dyes having bulky boryl groups in the side position of fluorophore skeleton inhibit close packing of the molecules that causes fluorescence quenching.[8] In other cases, Langhals et al. and Moorthy et al. showed that the introduction of bulky groups to perylene and pyrene skeletons can efficiently inhibit the close packing of their fluorescent molecules.[9,10] On the other hand, Ma et al. demonstrated that strong supramolecular interaction inducing tight packing and rigid molecules without parallel stacking in crystals of cyano substituent oligo(*para*-phenylene vinylene) are the key factor for the high luminescence efficiency of its crystals.[11] Consequently, it was confirmed that fluorophores **4** and **7** with bulky 5,5- and 3,3-dibutyl substituents have a nonconjugated linkage to the fluorophore skeleton.

In a previous paper, we reported the synthesis of heterocyclic quinols, 5-hydroxy-5-substituent-benzo[*b*]naphtho-[1,2-*d*]furan-6-one (**1a**–**c**), and 3-hydroxy-3-substituent-benzo[*kl*]xanthen-2-one (**2a**–**c**) fluorophores with substituents (R = Me, Bu, and Ph) having a nonconjugated linkage to the chromophores and their absorption and fluorescence properties in solution and in the solid state (Scheme 1).[4c] Dramatic substituent effects on the solid-state photophysical properties were observed, which were elucidated by means of X-ray crystallographic analysis. It was confirmed that the introduction of 5- and 3-substituents having a nonconjugated linkage to the chromophore skeletons of **1** and **2** can efficiently prevent the short π–π contact between the fluorophores in molecular aggregation states and thus cause

[‡] Heterocyclic Quinol-type Fluorophores, 8. Part 7: Y. Ooyama, K. Yoshida, *Eur. J. Org. Chem.*, DOI: 10.1002/ejoc.200800045.

[a] Department of Material Science, Faculty of Science, Kochi University,
Akebono-cho, Kochi 780-8520, Japan
Fax: +81-88-844-8359
E-mail: kyoshida@cc.kochi-u.ac.jp
yooyama@hiroshima-u.ac.jp

a dramatic solid-state fluorescence enhancement. On the basis of the results, the introduction of bulky 5,5-disubstituents and 3,3-disubstituents to the chromophore skeletons of **1** and **2**, respectively, would be expected to be more effective for the improvement of the solid-state fluorescence of these fluorophores. In this paper, we report the photophysical properties in solution and in the crystalline state of heterocyclic fluorophores 5,5-dibutyl-9-dibutylamino-5*H*-benzo[*b*]naphtho[1,2-*d*]furan-6-one (**4**) and 3,3-dibutyl-9-dibutylamino-3*H*-benzo[*kl*]xanthen-2-one (**7**) with bulky 5,5- and 3,3-dibutylsubstituents having a nonconjugated linkage to the fluorophore skeleton, respectively. To elucidate the dramatic effect of the dialkyl substituents on the solid-state fluorescence excitation and emission spectra, we performed X-ray crystallographic analysis.

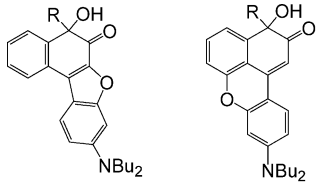

1a: R = Me
1b: R = Bu
1c: R = Ph

2a: R = Me
2b: R = Bu
2c: R = Ph

Scheme 1. Heterocyclic quinol-type fluorophores **1a**–**c** and **2a**–**c**.

Results and Discussion

Synthesis of 5,5-Dibutyl-9-dibutylamino-5*H*-benzo[*b*]-naphtho[1,2-*d*]furan-6-one (4) and 3,3-Dibutyl-9-dibutylamino-3*H*-benzo[*kl*]xanthen-2-one (7) Fluorophores

As shown in Scheme 2, we used 5-hydroxy-5-substituent-benzo[*b*]naphtho[1,2-*d*]furan-6-one (**1b**) and 3-hydroxy-3-substituent-benzo[*kl*]xanthen-2-one (**2b**) as starting materials.[4c] The reduction of **1b** and **2b** by using Zn in acetic acid was found to give **3** and **6**, respectively. Next, heterocyclic fluorophores **4** and **7** were easily obtained by reaction of **3** and **6** with iodobutane by using *tert*-butoxylithium, respectively.

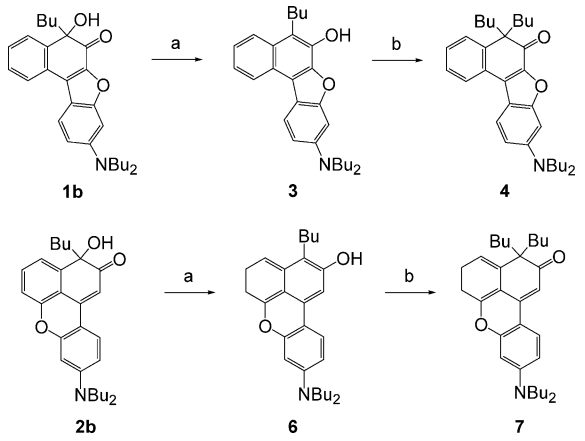

Scheme 2. Synthesis of **4** and **7**. Reagents and conditions: (a) Zn, CH_3COOH, reflux, 2–6 h; (b) *t*BuOLi, *n*BuI, 130 °C, 20 h, 57% for **4**, 25% for **7**.

Spectroscopic Properties of 1a–c, 2a–c, 4 and 7 in Solution

The visible absorption and fluorescence spectroscopic data of **4** and **7** in solution are summarized in Table 1, along with those of **1a**–**c** and **2a**–**c**. The fluorescence spectra of the compounds were recorded by excitation at the wavelengths of the longest absorption maximum. Fluorophore **4** exhibits an intense absorption band at around 410 nm and an intense fluorescence band at around 451 nm in 1,4-dioxane, which are blueshifted by 10 and 25 nm, respectively, relative to the absorption band and fluorescence band of **1b** in 1,4-dioxane. The fluorescence quantum yield (Φ) of **4** (Φ = 0.74) is similar to those of quinols **1a**–**c**. The absorption spectrum of **4** is little affected by increasing the solvent polarity from 1,4-dioxane to acetonitrile, whereas the fluorescence spectrum shows a large bathochromic shift and a reduction in fluorescence intensity, which was similar to the photophysical properties of quinols **1a**–**c**. On the other hand, fluorophore **7** exhibits intense absorption bands at around 407 and 427 nm and a weak fluorescence band at around 449 nm (Φ = 0.02) in 1,4-dioxane, which are blueshifted by 10, 7, and 16 nm, respectively, relative to the absorption band and fluorescence band of **2b** in 1,4-dioxane. In acetonitrile, fluorophore **7** exhibits intense absorption bands at around 412 and 430 nm and an intense fluorescence band at around 478 nm (Φ = 0.46). The longest absorption maximum of **7** shows a small bathochromic shift of 3 nm from 1,4-dioxane to acetonitrile, whereas the fluorescence maximum shows a large bathochromic shift of 29 nm. Significant dependence of the fluorescence quantum yield (Φ) on the solvent polarity was also observed: the Φ value of **7** is increased 23-fold by changing the solvent from 1,4-dioxane to acetonitrile. Similar fluorescence characteristics were previously reported in some aromatic carbonyl compounds such as pyrene-3-carboxaldehyde,[12] 7-alkoxycoumarins,[13] and *o*-aminoacetophenone.[14]

From the above results, owing to the nonconjugated linkage of the substituents (R = Me, Bu, and Ph) to the chromophore skeleton, the absorption and fluorescence spectra of fluorophores **1a**–**c** and **2a**–**c** are very similar in each category. However, hypsochromic shifts were observed in the absorption and fluorescence spectra of fluorophores **4** and **7** in comparison to those of **1a**–**c** and **2a**–**c**, respectively. The hypsochromic shift in the fluorescence spectra is larger than that in the absorption spectra. These results indicate that the differences in the fluorescence spectra between fluorophores **1a**–**c** and **4** or **2a**–**c** and **7** depend on the formation of intramolecular hydrogen bonds. The formation of intramolecular hydrogen bonds is possible for fluorophores **1a**–**c** and **2a**–**c**, but is not for fluorophores **4** and **7**. A large bathochromic shift in the fluorescence spectra induced by intramolecular hydrogen bonding was previously reported in a fluorophore such as 4-(4-hydroxybenzylidene)-1,2-dimethyl-1*H*-imidazole-5(4*H*)-one.[15] On the other hand, the

Table 1. Absorption and fluorescence spectroscopic data of **1a**–**c**, **2a**–**c**, **4**, and **7** in solution.

	Solvent	Absorption	Fluorescence		SS[a]
		λ_{max} [nm] (ε_{max} [$M^{-1}cm^{-1}$])	λ_{max} [nm]	Φ	$\Delta\lambda_{max}$ [nm]
1a	Benzene	427 (22500)	470	0.76	43
	1,4-Dioxane	421 (21300)	476	0.74	55
	THF	419 (20900)	494	0.60	75
	DMF	426 (20200)	524	0.35	98
	DMSO	430 (20400)	528	0.31	98
	Acetonitrile	428 (20500)	524	0.30	96
	Ethanol	432 (20400)	538	0.16	106
1b	1,4-Dioxane	420 (21700)	476	0.74	56
	Acetonitrile	430 (22600)	525	0.31	95
1c	1,4-Dioxane	430 (21600)	484	0.74	55
	Acetonitrile	441 (22400)	536	0.30	95
4	1,4-Dioxane	410 (25200)	451	0.73	41
	THF	409 (24700)	464	0.56	55
	Acetonitrile	415 (24100)	497	0.27	82
2a	Cyclohexane	430(30200), 408(32500)	441	0.03	11
	Diethyl ether	430(28400), 411(31300)	457	0.04	27
	1,4-Dioxane	433(29400), 416(28200)	464	0.04	31
	THF	433(29700), 419(31100)	479	0.14	46
	DMF	438(29200)	503	0.27	65
	DMSO	441(28700)	506	0.27	65
	Acetonitrile	438(32600)	501	0.46	63
	Ethanol	442(33200)	508	0.33	66
2b	1,4-Dioxane	434(29000), 417(28000)	465	0.04	31
	Acetonitrile	440(32400)	501	0.43	61
2c	1,4-Dioxane	442(31200), 426(30700)	472	0.03	30
	Acetonitrile	450(35300)	507	0.43	57
7	1,4-Dioxane	427(32100), 407(34600)	449	0.02	22
	THF	427(30300), 408(32300)	455	0.08	28
	Acetonitrile	430(32200), 412(32400)	478	0.46	48

[a] Stokes shift value.

methoxy derivative, 4-(4-methoxybenzylidene)-1,2-dimethyl-1 *H*-imidazole-5(4*H*)-one, which cannot form intramolecular hydrogen bonds, emits in the hypsochromic region in comparison to the above hydroxy compound.

Semiempirical MO Calculations (AM1, INDO/S) of 1a–c, 2a–c, 4, and 7

The photophysical spectra of compounds **1a**–**c**, **2a**–**c**, **4**, and **7** were analyzed by using semiempirical molecular orbital (MO) calculations. The molecular structures were optimized by using the MOPAC/AM1 method,[16] and then the INDO/S method[17] was used for spectroscopic calculations. The calculated absorption wavelengths and the transition character of the first absorption bands are collected in Table 2. The calculated absorption wavelengths and the oscillator strength values are relatively well matched to the observed spectra in 1,4-dioxane, although the calculated absorption spectra are blueshifted. The deviation in the INDO/S calculations, giving transition energies greater than the experimental values, has been generally observed.[18] The calculations explain well that the calculated absorption spectra of quinols **1a**–**c** or **2a**–**c** resemble each other very well, because of the nonconjugated linkage of the substituents (R = Me, Bu, and Ph) to the chromophore skeleton. The calculated absorption wavelengths of **4** and **7** are blueshifted relative to those of **1a**–**c** and **2a**–**c**, respectively, which is compatible with the observed spectra in solution. Furthermore, the calculated oscillator strengths (*f*) of compounds **1a**–**c** and **4** or **2a**–**c** and **7** are almost identical in each category, which is also compatible with the observed spectra in solution.

Table 2. Calculated absorption spectra for compounds **1a**–**c**, **2a**–**c**, **4**, and **7**.

Quinol	μ	Absorption (calcd.)		CI component (%)[c]	$\Delta\mu$
	[D][a]	λ_{max} [nm]	f [b]		[D][d]
1a	7.35	362	0.48	HOMO→LUMO (89)	7.52
1b	6.17	367	0.42	HOMO→LUMO (89)	5.91
1c	6.98	355	0.46	HOMO→LUMO (89)	7.23
4	6.52	353	0.48	HOMO→LUMO (88)	6.10
2a	7.21	342	0.74	HOMO→LUMO (86)	6.47
2b	7.03	343	0.74	HOMO→LUMO (86)	6.32
2c	7.10	346	0.71	HOMO→LUMO (86)	5.93
7	6.34	335	0.74	HOMO→LUMO (86)	6.24

[a] The values of the dipole moment in the ground state. [b] Oscillator strength. [c] The transition is shown by an arrow from one orbital to the other, followed by its percentage CI (configuration interaction) component. [d] The values of the difference in the dipole moment between the excited and the ground states.

For compounds **1a**–**c** and **4**, the calculations show that the longest excitation bands for the four compounds are mainly assigned to the transition from the HOMO to the LUMO, where the HOMO were mostly localized on the *p*-

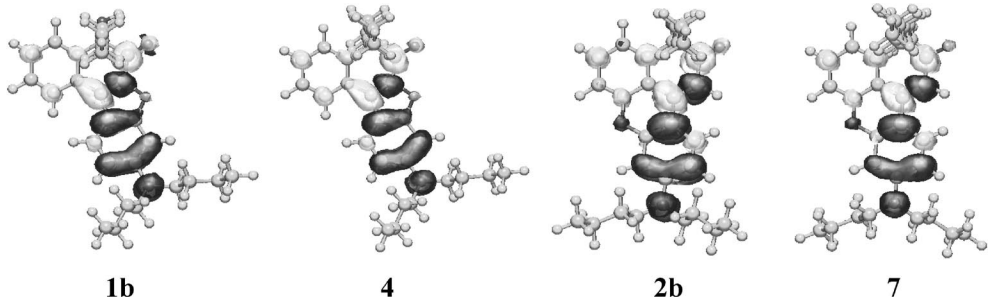

Figure 1. Calculated electron density changes accompanying the first electronic excitation of **1b**, **2b**, **4**, and **7**. The black and white lobes signify the decrease and increase in electron density accompanying the electronic transition. Their areas indicate the magnitude of the electron density change.

dibutylaminobenzofurano moiety and the LUMO were mostly localized on the naphthoquinol moiety. On the other hand, for compounds **2a**–**c** and **7**, the calculations also show that the longest excitation bands for the four compounds are mainly assigned to the transition from the HOMO to the LUMO, where the HOMO are mostly localized on the *p*-dibutylaminobenzopyran moiety and the LUMO were mostly localized on the naphthoquinol moiety. The calculated electron density changes accompanying the first electron excitation are shown in Figure 1, which shows a strong migration of intramolecular charge-transfer character of **1a**–**c**, **2a**–**c**, **4**, and **7**.

The values of the dipole moments in the grand states are 7.35 for **1a**, 6.17 for **1b**, 6.98 for **1c**, 6.52 for **4**, 7.21 for **2a**, 7.03 for **2b**, 7.10 for **2c**, and 6.34 for **7**. The differences between the dipole moments ($\Delta\mu$) of the first excited and the ground states are 7.52 for **1a**, 5.91 for **1b**, 7.23 for **1c**, and 6.10 for **4**, 6.47 for **2a**, 6.32 for **2b**, 5.93 for **2c**, and 6.24 for **7**. These calculations indicate that compounds **1a**–**c** and **4** or **2a**–**c** and **7** have similar large dipole moments in the excited state, which well explains the experimental observations that these compounds show a large bathochromic shift in their fluorescence maxima in polar solvents and that the Stokes shift values for the these compounds in acetonitrile are much larger than those in 1,4-dioxane.

Spectroscopic Properties of 1a–c, 4, 2a–c, and 7 in the Solid State

Interesting results were obtained by comparing the photophysical properties of the crystals of **4** and **7** with those of the crystals of **1a**–**c** and **2a**–**c**. Figure 2 shows that the optical properties of **1a**–**c** and **4** or **2a**–**c** and **7** are quite different between the solution and the solid state. The crystal of **4** exhibits strong blue fluorescence emission, but the crystals of **1a**, **1b**, and **1c** exhibit relatively weak yellowish-orange, green, and greenish-yellow fluorescence emission, respectively. On the other hand, the crystal of **7** exhibits strong greenish-yellow emission, whereas the crystals of **2a**, **2b**, and **2c** exhibit relatively weak yellowish-orange, green, and red emissions, respectively. In order to investigate the difference in the solid-state photophysical properties among **1a**–**c** and **4** or **2a**–**c** and **7**, we measured the fluorescence excitation and emission spectra of the crystals. Figures 3 and 4 show the spectroscopic properties of **1a**–**c** and **4** or **2a**–**c** and **7** in the crystalline state. The fluorescence intensity of **1a**–**c** and **4** are in the order of **4** > **1c** > **1b** > **1a** in the crystalline state: the fluorescence intensity of **4** is ca. fivefold larger than that of **1b**. The wavelengths of the emission maximum of **1a** (λ_{em} = 560 nm), **1b** (λ_{em} = 530 nm), **1c** (λ_{em} = 555 nm), and **4** (λ_{em} = 480 nm) are redshifted by 84, 54, 70, and 29 nm, respectively, relative to that in 1,4-dioxane. It is noteworthy that the emission maximum of **4** in the solid state is similar to that in 1,4-dioxane.

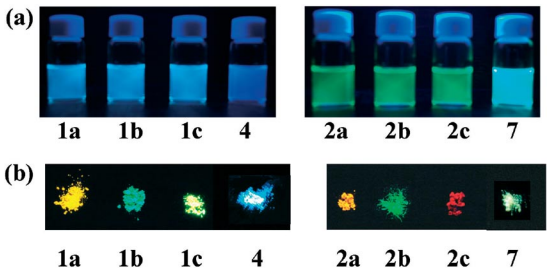

Figure 2. Fluorescence properties of **1a**–**c**, **2a**–**c**, **4**, and **7** (a) in solution (1,4-dioxane for **1a**–**c** and **4**; DMSO for **2a**–**c** and **7**) and (b) in the solid state.

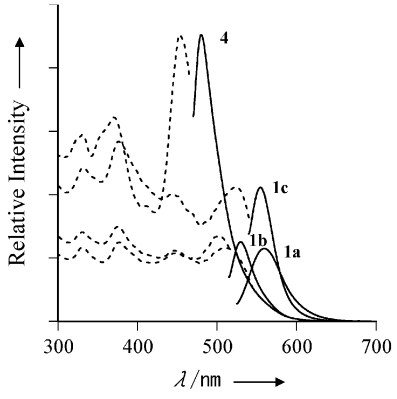

Figure 3. Solid-state excitation (···) and emission (—) spectra of the crystals of **1a**–**c** and **4**; **1a**: λ_{ex} = 510 nm, λ_{em} = 560 nm; **1b**: λ_{ex} = 503 nm, λ_{em} = 530 nm; **1c**: λ_{ex} = 519 nm, λ_{em} = 555 nm; **4**: λ_{ex} = 454 nm, λ_{em} = 480 nm.

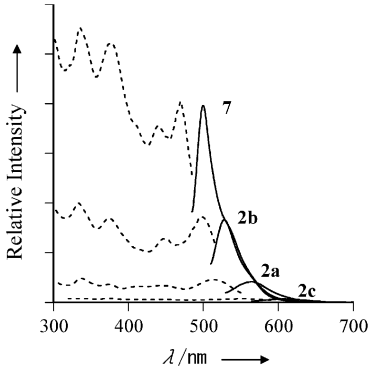

Figure 4. Solid-state excitation (···) and emission (−) spectra of the crystals of **2a**–**c** and **7**; **2a**: λ_{ex} = 514 nm, λ_{em} = 564 nm; **2b**: λ_{ex} = 497 nm, λ_{em} = 529 nm; **2c**: λ_{ex} = 550 nm, λ_{em} = 608 nm; **7**: λ_{ex} = 470 nm, λ_{em} = 500 nm.

On the other hand, the fluorescence intensity of **2a**–**c** and **7** are in the order of **7** > **2b** > **2a** > **2c** in the crystalline state. The longest wavelengths of the excitation and the emission maxima of **7** (λ_{ex} = 470 nm, λ_{em} = 500 nm) in the crystalline state are redshifted by 43 and 51 nm, respectively, relative to those of **7** in 1,4-dioxane. In contrast, the longest wavelengths of the excitation and the emission maxima of **2b** (λ_{ex} = 497 nm, λ_{em} = 529 nm) in the crystalline state are largely redshifted by 63 and 64 nm, respectively, relative to those of **2b** in 1,4-dioxane. These results demonstrated that the solid-state photophysical properties of **4** and **7** having dialkyl substituent approach their photophysical properties in solution.

X-ray Crystal Structures of 1a–c, 4, 2a–c, and 7

In a previous paper, we demonstrated that the substituents (R = Me, Bu, Ph) of quinols **1a**–**c** and **2a**–**c** greatly affect the geometric arrangement in the crystal structure.[4c] In **1a**, **1b**, and **2c**, the interplanar distance between the fluorophores is short because the substituent (methyl group in **1a**, butyl group in **1b**, and phenyl group in **2c**) and the 9-dibutylamino group are located on the same side of the π plane, and the molecules are packed in the structural form with a table shape (Figure 9). The large redshift in the absorption and fluorescence maxima and the solid-state fluo-

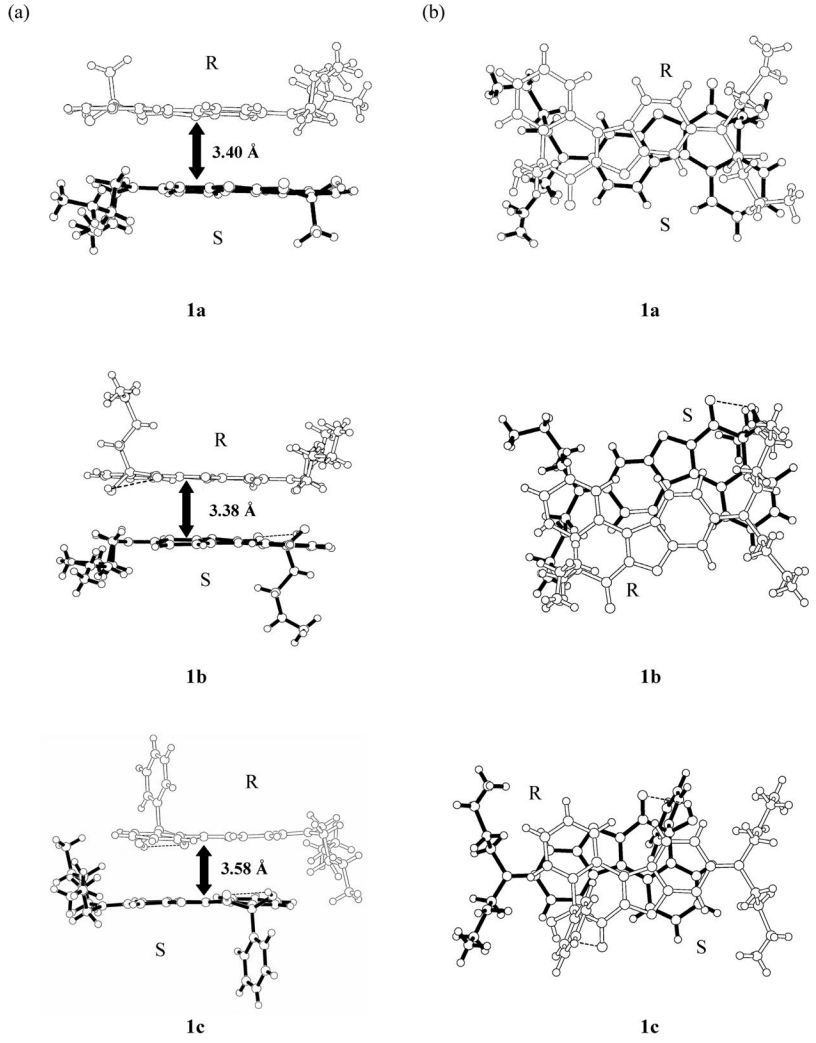

Figure 5. Crystal packing pattern of **1a**–**c**: (a) a side view and (b) a top view of the pairs of fluorophores.

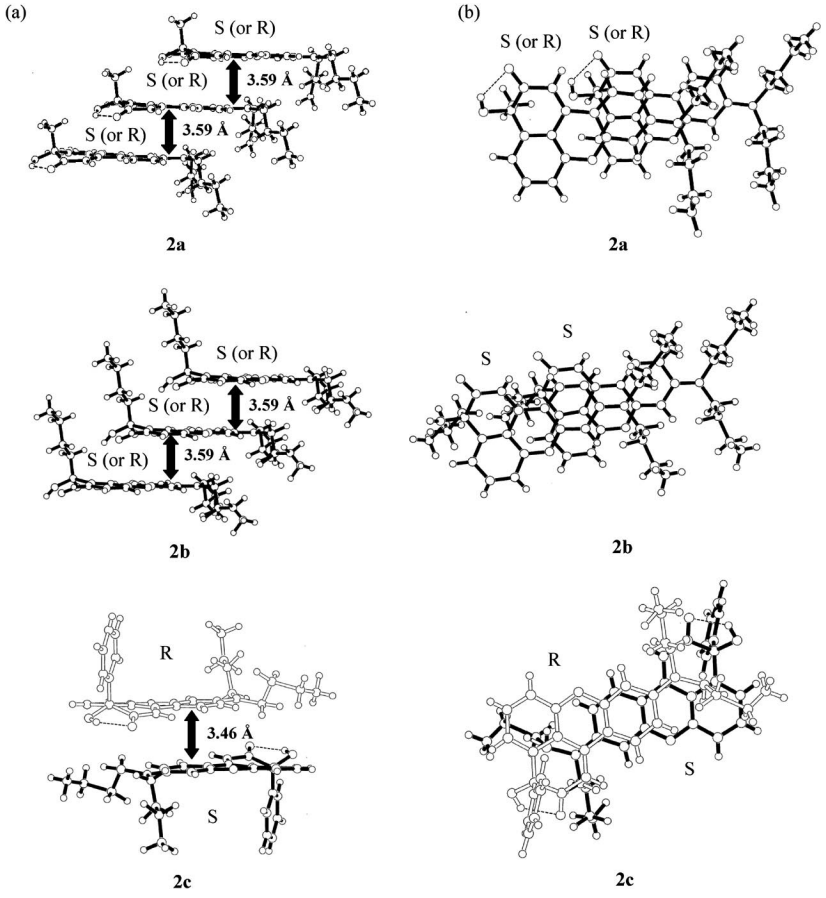

Figure 6. Crystal packing pattern of **2a**–**c**: (a) a side view and (b) a top view of the pairs of fluorophores.

rescence quenching in the crystals of **1a** and **2c** are considered to be induced by strong donor–acceptor-type π–π interactions.[3f,4,5] On the other hand, in **1c**, **2a**, and **2b**, the molecules are packed in the structural form with a stepped-shape, because the substituent (phenyl group in **1c**, methyl group in **2a**, and butyl group in **2b**) and the 9-dibutylamino group are located on opposite sides of the molecular π plane (Figures 5 and 6). Therefore, the interplanar distance between the fluorophores is longer (Figure 9) so that the π–π interactions are weakened by the substituents, which thus leads to a stronger solid-state fluorescence emission.

From these results, the introduction of bulky 5,5-disubstituents and 3,3-disubstituents to the chromophore skeletons of **1** and **2**, respectively, should more efficiently prevent the short π–π contact between the fluorophores in the molecular aggregation states. To elucidate the dramatic substituent effect on the solid-state photophysical properties, the X-ray crystal structures of **4** and **7** were determined and they are shown in Figures 7 and 8, respectively. The crystal systems of these compounds are summarized in Table 3. The packing structures demonstrate that the molecules are arranged in a "herring-bone" fashion in the crystals of both **4** and **7**. In the case of the two dialkyl derivatives, there are no intermolecular hydrogen bonds between the enantiomers. As we expected, the crystal structure of **4** has only one edge-to-edge interatomic contact [O(1)···C(77) 3.207(4) Å] of less than 3.60 Å between the neighboring fluorophores in the crystal structure (Figure 7). In the crystal of **7**, on the other hand, a π stacking of the fluorophores was formed in one cluster unit, in which partial π overlappings were observed between the chromene moiety and the 9-dibutylaminobenzo moiety of the adjacent fluorophores. The inclination between the benzoxanthenone planes in the pair of equal enantiomers is 17° [Figure 8(c)]. Furthermore, continuous π stacking of the equal enantiomers formed in the crystal structures of **2a** and **2b** and strong donor–acceptor π stacking formed in the crystal structures of **2c** were not observed in the crystal structure of **7**. As evident by comparing the crystal structure of **7** with those of **2a**–**c**, the range of π stacking in **7** is much less than that in **2a**–**c**. These results demonstrate that the introduction of dialkyl substituents to fluorophores effectively prevents intermolecular π–π interactions and intermolecular hydrogen bonding between fluorophores, which causes a large redshift in the absorption and fluorescence maxima and fluorescence quenching in the solid state.

In the crystals of **4** and **7**, the molecules are packed in the structural form with a chair shape. Therefore, the interplanar distance between the fluorophores is longer (Figure 9), so that the π–π interactions are weakened by the substituents, which leads to stronger solid-state fluorescence emission. From these results, we propose a favorable stereo-

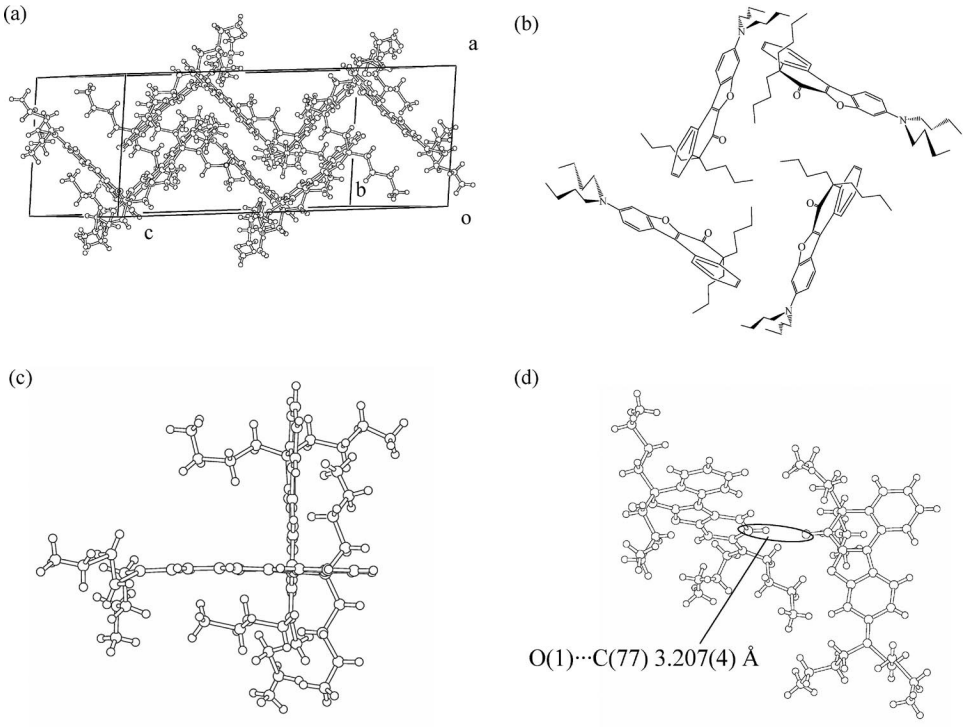

Figure 7. Crystal packing of **4**: (a) a stereoview of the molecular packing structure, (b) a schematic structure, (c) a side view, and (d) a top view of the pairs of fluorophores.

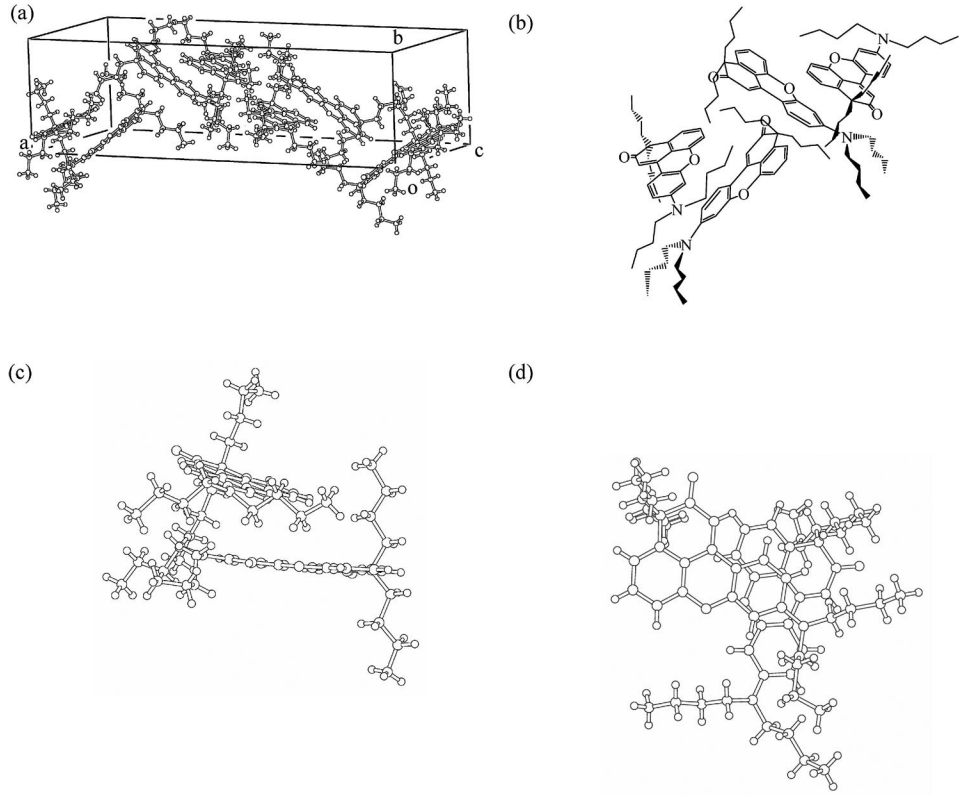

Figure 8. Crystal packing of **7**: (a) a stereoview of the molecular packing structure, (b) a schematic structure, (c) a side view, and (d) a top view of the pairs of fluorophores.

Table 3. Crystal data and structure refinement parameters for compounds **4** and **7**.

Compound	**4**	**7**
Molecular formula	$C_{32}H_{43}NO_2$	$C_{32}H_{43}NO_2$
Formula weight	473.70	473.70
Number of reflections for unit cell Cell determination (2θ range [°])	23 (25.0–33.0)	16 (22.2–24.2)
Crystal system	triclinic	monoclinic
Space group	$P\bar{1}$	$P2_1/n$
a [Å]	11.689(2)	37.767(8)
b [Å]	17.905(7)	11.080(4)
c [Å]	28.309(5)	14.074(4)
a/°	79.75(2)	
β [°]	93.56(2)	98.74(2)
γ [°]	95.65(3)	
V [Å^3]	5795(2)	5820(3)
Z	8	8
$D_{calcd.}$ [g cm^{-3}]	1.086	1.081
$F(000)$	2064.00	2064.00
M (Mo-K_α) [cm^{-1}]	0.66	0.66
Crystal dimensions [nm]	$0.80 \times 0.66 \times 0.43$	$0.55 \times 0.35 \times 0.50$
Scan mode	ω-2θ	ω–2θ
Scan rate in ω[°min^{-1}]	8.0–16.0 (up to 5 scans)	8.0–16.0 (up to 7 scans)
Scan wide [°]	1.47 + 0.30tanθ	1.21 + 0.30tanθ
2θ max [°]	55.0	50.0
Range of induces h; k; l	0, 15; –23, 23; –36, 36	0, 44; –13, 0; –16, 16
Reflection collected (unique)	26601	10238
Reflection observed with $I_0 > 2\sigma I_0$	6697	3491
Number of parameters	1262	632
R	0.063	0.060
Rw	0.144	0.179
W	$(\sigma^2 F^2)^{-1}$	$(\sigma^2 F^2)^{-1}$
S	1.26	1.25
Max. Shift/Error in final cycle	0.029	0.015
Max. Peak in final diff. map [e Å^{-3}]	0.54	0.27
Min. Peak in final diff. map [e Å^{-3}]	–0.55	–0.23

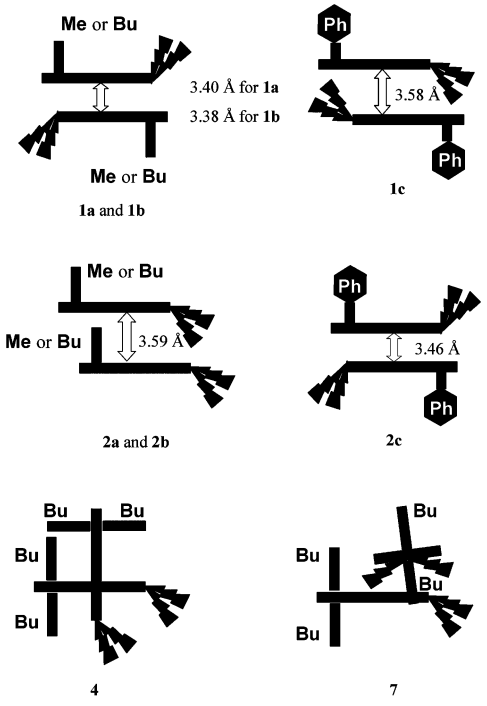

Figure 9. Schematic representation of the effects of the substituents on interplanar distances between a pair of fluorophores for **1a**–**c**, **2a**–**c**, **4**, and **7**.

structure for the solid-state fluorescence. For example, the H-shaped fluorophores with four bulky substituents located on both sides of the π plane, which leads to inhibition of the π–π interactions between the fluorophores, would exhibit strong fluorescence in the solid state, but it would also exhibit almost the same fluorescence properties in solution as it would in the solid state.

Conclusions

We synthesized the heterocyclic fluorophores 5,5-dibutyl-9-dibutylamino-5*H*-benzo[*b*]naphtho[1,2-*d*]furan-6-one (**4**) and 3,3-dibutyl-9-dibutylamino-3*H*-benzo[*kl*]xanthen-2-one (**7**) having bulky dialkyl substituents linked in a nonconjugated fashion to the chromophore skeleton have been derived from the quinol-type compounds **1** and **2**, and their photophysical properties were investigated in solution and in the solid state. Dramatic dialkyl substituent effects on the solid-state photophysical properties were observed, and these effects were elucidated by means of X-ray crystallographic analysis. It was confirmed that fluorophores **4** and **7** with bulky 5,5- and 3,3-dibutylsubstituents having a nonconjugated linkage to the fluorophore skeleton can efficiently prevent the short π–π contact between the fluorophores causing fluorescence quenching in the solid state.

Experimental Section

General: Melting points were measured with a Yanaco micromelting point apparatus MP-500D. IR spectra were recorded with a JASCO FTIR-5300 spectrophotometer for samples in KBr pellet form. Absorption spectra were observed with a JASCO U-best30 spectrophotometer and fluorescence spectra were measured with a JASCO FP-777 spectrophotometer. Single-crystal X-ray diffraction was performed with a Rigaku AFC7S diffractometer. For the measurement of the solid-state fluorescence excitation and emission spectra of the crystals, a JASCO FP-777 spectrometer equipped with a JASCO F*P*-1060 attachment was used. The fluorescence quantum yields (Φ) for **1a**–**c** and **2a**–**c** were determined by using 9,10-bis(phenylethynyl)anthracene (Φ = 0.84, λ_{ex} = 440 nm)[19] in benzene as the standard. The fluorescence quantum yields (Φ) for **4** and **7** were determined by using 9,10-diphenylanthracene (Φ = 0.67, λ_{ex} = 357 nm)[19] in benzene as the standard. Elemental analyses were recorded with a Perkin–Elmer 2400 II CHN analyzer. ^{1}H NMR spectra were recorded with a JNM-LA-400 (400 MHz) FT NMR spectrometer with tetramethylsilane (TMS) as an internal standard. Column chromatography was performed on silica gel (KANTO CHEMICAL, 60*N*, spherical, neutral).

5,5-Dibutyl-9-dibutylamino-5*H*-benzo[*b*]naphtho[1,2-*d*]furan-6-one (4): A solution of **1b** (0.70 g, 1.61 mmol) and Zn powder (1.29 g, 24.2 mmol) in acetic acid (70 mL) was heated at reflux for 6 h. The reaction mixture was filtered, and the filtrate was evaporated. The residue was extracted with CH_2Cl_2. The organic extract was washed with water. Evaporation of the solvent afforded **3** as a white solid, which is unstable in air. A mixture of **3**, iodobutane (2.97 g, 16.1 mmol), and *tert*-butoxylithium (1.42 g, 17.8 mmol) was stirred at 130 °C for 20 h. The reaction mixture was extracted with CH_2Cl_2. The organic extract was washed with water and neutralized with NH_4Cl aqueous solution. The organic extract was evaporated, and the residue was chromatographed on silica gel (CH_2Cl_2) to give **4** (0.44 g, yield 57%) as a yellow powder. Data for crude **3**: ^{1}H NMR (400 MHz, [D$_6$]acetone, TMS): δ = 0.94–1.72 (m, 21 H), 3.25 (t, J = 7.8 Hz, 2 H), 3.48 (t, J = 7.6 Hz, 4 H), 6.84–6.86 (m, 2 H), 6.74–6.76 (m, 2 H), 8.02–8.16 (m, 2 H), 8.44–8.47 (m, 1 H) ppm. Data for **4**: M.p. 149–150 °C. ^{1}H NMR (400 MHz, [D$_3$]chloroform, TMS): δ = 0.60–1.16 (m, 24 H), 1.34–1.43 (m, 4 H), 1.57–1.67 (m, 4 H), 1.82–2.38 (m, 4 H), 3.47 (t, J = 7.32 Hz, 4 H), 6.76 (d, J = 2.2 Hz, 1 H), 6.82 (dd, J = 9.0, 2.2 Hz, 1 H), 7.40–7.50 (m, 4 H), 8.01 (d, J = 9.0 Hz, 1 H) 8.10 (dd, 1 H, J = 6.6, 2.44 Hz) ppm. IR (KBr): $\tilde{\nu}$ = 1617 cm^{-1}. $C_{32}H_{43}NO_2$ (473.69): calcd. C 81.14, H 9.15, N 2.96; found C 81.33, H 9.16, N 2.92.

3,3-Dibutyl-9-dibutylamino-3*H*-benzo[*kl*]xanthen-2-one (7): A solution of **2b** (1.59 g, 3.67 mmol) and Zn powder (3.62 g, 55.0 mmol) in acetic acid (150 mL) was heated at refluxed for 2 h. The reaction mixture was filtered, and the filtrate was evaporated. The residue was extracted with CH_2Cl_2. The organic extract was washed with water. Evaporation of the solvent afforded **6** as a white solid, which is unstable in air. A mixture of **6**, iodobutane (6.75 g, 36.7 mmol), and *tert*-butoxylithium (4.40 g, 55.0 mmol) was stirred at 130 °C for 20 h. The reaction mixture was extracted with CH_2Cl_2. The organic extract was washed with water and neutralized with NH_4Cl aqueous solution. The organic extract was evaporated and the residue was chromatographed on silica gel (CH_2Cl_2) to give **7** (0.44 g, yield 25%) as a yellow powder. Data for crude **6**: ^{1}H NMR (400 MHz, [D$_3$]chloroform, TMS): δ = 0.95–1.68 (m, 21 H), 2.86 (t, J = 7.8 Hz, 2 H), 3.36 (t, J = 7.8 Hz, 4 H), 6.40–6.61 (m, 2 H), 6.67–6.77 (m, 1 H), 6.98–7.06 (m, 1 H), 7.27–7.43 (m, 3 H) ppm. Data for **7**: M.p. 111–112 °C. ^{1}H NMR (400 MHz, [D$_6$]acetone, TMS): δ = 0.68–1.17 (m, 16 H), 1.38–1.70 (m, 12 H), 1.82–2.12 (m, 4 H), 3.50 (t, J = 7.6 Hz, 4 H), 6.33 (s, 1 H), 6.47 (d, J = 2.44 Hz, 1 H), 6.79 (dd, J = 2.44, 9.04 Hz, 1 H), 7.16 (d, J = 8.0 Hz, 1 H), 7.36 (d, J = 8.0 Hz, 1 H), 7.57 (t, J = 8.0 Hz, 1 H),7.84 (d, J = 9.04 Hz, 2 H) ppm. IR (KBr): $\tilde{\nu}$ = 1597 cm^{-1}. $C_{32}H_{43}NO_2$ (473.69): calcd. C 81.14, H 9.15, N 2.96; found C 81.42, H 9.39, N 2.93.

X-ray Crystallographic Studies: The reflection data were collected at 23 ± 1 °C with a Rigaku AFC7S four-circle diffractometer by 2θ-ω scan technique and by using graphite-monochromated Mo-K_α (λ = 0.71069 Å) radiation at 50 kV and 30 mA. In all case, the data were corrected for Lorentz and polarization effects. A correction for secondary extinction was applied. The reflection intensities were monitored by three standard reflections for every 150 reflections. An empirical absorption correction based on azimuthal scans of several reflections was applied. All calculations were performed using the teXsan[20] crystallographic software package of Molecular Structure Corporation. CCDC-294660 (for **1a**), -294661 (for **1b**), -294662 (for **1c**) -294192 (for **2a**), -294193 (for **2b**), -294194 (for **2c**), -652309 (for **4**), and -652310 (for **7**) contain the supplementary crystallographic data for this paper. These data can be obtained free of charge from The Cambridge Crystallographic Data Centre via www.ccdc.cam.ac.uk/data_request/cif.

Compound 4: Crystals of **4** were recrystallized from *n*-hexane and obtained as air-stable, yellow prisms. The one selected had approximate dimensions of 0.80 × 0.66 × 0.43 mm. The transmission factors ranged from 0.93 to 1.00. The crystal structure was solved by direct methods by using SIR 92.[21] The structures were expanded by using Fourier techniques.[22] The non-hydrogen atoms were refined anisotropically. Some hydrogen atoms were refined isotropically, the rest were fixed geometrically and not refined. Crystal data: $C_{32}H_{43}NO_2$, M = 473.70, triclinic, a = 11.689(2) Å, b = 17.905(7) Å, c = 28.309(5) Å, α = 79.75(2)°, β = 93.56(2)°, γ = 95.65(2)°, U = 5795(2) Å^3, T = 296.2 K, space group $P\bar{1}$ (no. 2), Z = 8, μ(Mo-K_α) = 0.66 cm^{-1}, 27900 reflections measured, 26601 unique (R_{int} = 0.024), which were used in all calculations. The final R indices [$I > 2\sigma(I)$], R_1 = 0.063, $wR(F^2)$ = 0.144.

7: Crystals of **7** were recrystallized from *n*-hexane and obtained as air-stable, yellow prisms. The one selected had approximate dimensions of 0.55 × 0.35 × 0.50 mm. The transmission factors ranged from 0.93 to 1.00. The crystal structure was solved by direct methods by using SIR 92.[21] The structures were expanded by using Fourier techniques.[22] The non-hydrogen atoms were refined anisotropically. Some hydrogen atoms were refined isotropically, the rest were fixed geometrically and not refined. Crystal data: $C_{32}H_{43}NO_2$, M = 473.70, monoclinic, a = 37.767(8) Å, b = 11.080(2) Å, c = 14.074(4) Å, β = 98.74(2)°, U = 5820(3) Å^3, T = 296.2 K, space group $P2_1/n$ (no. 14), Z = 8, μ(Mo-K_α) = 0.66 cm^{-1}, 10990 reflections measured, 10238 unique (R_{int} = 0.059), which were used in all calculations. The final R indices [$I > 2\sigma(I)$], R_1 = 0.060, $wR(F^2)$ = 0.179.

Computational Methods: All calculations were performed with a FUJITSU FMV-ME4/657. The semiempirical calculations were carried out with the WinMOPAC Ver. 3 package (Fujitsu, Chiba, Japan). Geometry calculations in the ground state were carried out by using the AM1 method.[16] All geometries were completely optimized (keyword PRECISE) by the eigenvector following routine (keyword EF). Experimental absorption spectra of the compounds were studied with the semiempirical method INDO/S (intermediate neglect of differential overlap/spectroscopic).[17] All INDO/S calculations were performed by using single excitation full SCF/CI (self-consistent field/configuration interaction), which includes the configuration with one electron excited from any occupied orbital to

any unoccupied orbital, 225 configurations were considered for the configuration interaction [keyword CI (15 15)].

Acknowledgments

This work was partially supported by a Grant-in-Aid for Science and Research from the Ministry of Education, Science, Sport and Culture of Japan (Grant 18350100), by a Science and Technology Incubation Program in Advanced Regions of Japan Science and Technology Agency (JST), and by a Special Research Grant for Green Science from Kochi University.

[1] a) C. W. Tang, S. A. VansSlyke, *Appl. Phys. Lett.* **1987**, *51*, 913–915; b) C. W. Tang, S. A. VansSlyke, C. H. Chen, *J. Appl. Phys.* **1989**, *65*, 3610–3616; c) J. Schi, C. W. Tang, *Appl. Phys. Lett.* **1997**, *70*, 1665–1667; d) A. Kraft, A. C. Grimsdale, A. B. Holmes, *Angew. Chem.* **1998**, *110*, 416–443; *Angew. Chem. Int. Ed.* **1998**, *37*, 402–428; e) U. Mitschke, P. Bäuerle, *J. Mater. Chem.* **2000**, *10*, 1471–1507; f) K.-C. Wong, Y.-Y. Chien, R.-T. Chen, C.-F. Wang, Y.-T. Liu, H.-H. Chiang, P.-Y. Hsieh, C.-C. Wu, C. H. Chou, Y. O. Su, G.-H. Lee, S.-M. Peng, *J. Am. Chem. Soc.* **2002**, *124*, 11576–11577; g) C. J. Tonzola, M. M. Alam, W. K. Kaminsky, S. A. Jenekhe, *J. Am. Chem. Soc.* **2003**, *125*, 13548–13558; h) H.-C. Yeh, L.-H. Chan, W.-C. Wu, C.-T. Chen, *J. Mater. Chem.* **2004**, *14*, 1293–1298; i) C.-T. Chen, *Chem. Mater.* **2004**, *16*, 4389–4400; j) C.-L. Chiang, M.-F. Wu, D.-C. Dai, Y.-S. Wen, J.-K. Wang, C.-T. Chen, *Adv. Funct. Mater.* **2005**, *15*, 231–238; k) D. Berner, C. Klein, M. D. Nazeeruddin, F. de Angelis, M. Castellani, P. Bugnon, R. Scopelliti, L. Zuppiroli, M. Graetzel, *J. Mater. Chem.* **2006**, *16*, 4468–4474.

[2] a) Z.-S. Wang, F.-Y. Li, C.-H. Hang, L. Wang, M. Wei, L.-P. Jin, N.-Q. Li, *J. Phys. Chem. B* **2000**, *104*, 9676–9682; b) A. Ehret, L. Stuhl, M. T. Spitler, *J. Phys. Chem. B* **2001**, *105*, 9960–9965; c) K. Hara, T. Sato, R. Katoh, A. Furube, Y. Ohga, A. Shinpo, S. Suga, K. Sayama, H. Sugihara, H. Arakawa, *J. Phys. Chem. B* **2003**, *107*, 597–606; d) K. R. J. Thomas, J. T. Kin, Y.-C. Hsu, K.-C. Ho, *Chem. Commun.* **2005**, 4098–4100; e) D. P. Hagberg, T. Edvinsson, T. Marinado, G. Boschloo, A. Hagfeld, L. Sun, *Chem. Commun.* **2006**, 2245–2247; f) S.-L. Li, K.-J. Jiang, K.-F. Shao, L.-M. Yang, *Chem. Commun.* **2006**, 2792–2794.

[3] a) K. Hirano, S. Minakata, M. Komatsu, *Chem. Lett.* **2001**, 8–9; b) Y. Sonoda, Y. Kawanishi, T. Ikeda, M. Goto, S. Hayashi, N. Tanigaki, K. Yase, *J. Phys. Chem. B* **2003**, *107*, 3376–3383; c) R. Davis, S. Abraham, N. P. Rath, S. Das, *New J. Chem.* **2004**, *28*, 1368–1372; d) V. de Halleux, J.-P. Calbert, P. Brocorens, J. Cornil, J.-P. Declercq, J.-L. Brédas, Y. Geerts, *Adv. Funct. Mater.* **2004**, *14*, 649–659; e) H.-C. Yeh, W.-C. Wu, Y.-S. Wen, D.-C. Dai, J.-K. Wang, C.-T. Chen, *J. Org. Chem.* **2004**, *69*, 6455–6462; f) E. Horiguchi, S. Matsumoto, K. Funabiki, M. Matsui, *Bull. Chem. Soc. Jpn.* **2005**, *78*, 1167–1173; g) S. Mizukami, H. Houjou, K. Sugaya, E. Koyama, H. Tokuhisa, T. Sasaki, M. Kanesato, *Chem. Mater.* **2005**, *17*, 50–56; h) Y. Mizobe, N. Tohnai, M. Miyata, Y. Hasegawa, *Chem. Commun.* **2005**, 1839–1841; i) I. Vayá, M. C. Jiménez, M. Miranda, *Tetrahedron: Asymmetry* **2005**, *16*, 2167–2171; j) Z. Xie, B. Yang, L. Liu, M. li, D. Lin, Y. Ma, G. Cheng, S. Liu, *J. Phys. Org. Chem.* **2005**, *18*, 962–973; k) Y. Ooyama, Y. Harima, *Chem. Lett.* **2006**, 902–903; l) Y. Ooyama, Y. Kagawa, Y. Harima, *Eur. J. Org. Chem.* **2007**, 3613–3621.

[4] a) K. Yoshida, Y. Ooyama, M. Miyazaki, S. Watanabe, *J. Chem. Soc. Perkin Trans. 2* **2002**, 700–707; b) Y. Ooyama, T. Nakamura, K. Yoshida, *New J. Chem.* **2005**, *29*, 447–456; c) Y. Ooyama, T. Okamoto, T. Yamaguchi, T. Suzuki, A. Hayashi, K. Yoshida, *Chem. Eur. J.* **2006**, *12*, 7827–7838; d) Y. Ooyama, T. Mamura, K. Yoshida, *Tetrahedron Lett.* **2007**, *48*, 5791–5793; e) Y. Ooyama, T. Mamura, K. Yoshida, *Eur. J. Org. Chem.* **2007**, *30*, 5010–5019.

[5] a) K. Yoshida, J. Yamazaki, Y. Tagashira, S. Watanabe, *Chem. Lett.* **1996**, 9–10; b) K. Yoshida, T. Tachikawa, J. Yamasaki, S. Watanabe, S. Tokita, *Chem. Lett.* **1996**, 1027–1028; c) K. Yoshida, H. Miyazaki, Y. Miura, Y. Ooyama, S. Watanabe, *Chem. Lett.* **1999**, 837–838; d) K. Yoshida, Y. Ooyama, S. Tanikawa, S. Watanabe, *Chem. Lett.* **2000**, 714–715; e) K. Yoshida, Y. Ooyama, S. Tanikawa, S. Watanabe, *J. Chem. Soc. Perkin Trans. 2* **2002**, 708–714; f) Y. Ooyama, K. Yoshida, *New J. Chem.* **2005**, *29*, 12041212.

[6] H. Langhals, T. Potrawa, H. Nöth, G. Linti, *Angew. Chem.* **1989**, *101*, 497–499; *Angew. Chem. Int. Ed. Engl.* **1989**, *28*, 478–480.

[7] K. Yoshida, K. Uwada, H. Kumaoka, L. Bu, S. Watanabe, *Chem. Lett.* **2001**, 808–809.

[8] C.-H. Zhao, A. Wakamiya, Y. Inukai, S. Yamaguchi, *J. Am. Chem. Soc.* **2006**, *128*, 15934–15935.

[9] H. Langhals, R. Ismael, O. Yürük, *Tetrahedron* **2000**, *56*, 5435–5441.

[10] J. N. Moorthy, P. Natarajan, P. Venkatakrishnan, D.-F. Huang, T. J. Chow, *Org. Lett.* **2007**, *9*, 5215–5218.

[11] Y. Li, F. Li, H. Zhang, Z. Xie, W. Xie, H. Xu, B. Li, F. Shen, L. Ye, M. Hanif, D. Ma, Y. Ma, *Chem. Commun.* **2007**, 231–233.

[12] K. Kalyanasundaram, J. K. Thomas, *J. Phys. Chem.* **1977**, *81*, 2176–2180.

[13] B. Valeur, *Molecular Fluorescence*, VCH, Weinheim, **2002**.

[14] T. Yoshihara, H. Shimada, H. Shizuka, S. Tobita, *Phys. Chem. Chem. Phys.* **2001**, *3*, 4972–4978.

[15] K.-Y. Chen, Y.-M. Cheng, C.-H. Lai, C.-C. Hsu, M.-L. Ho, G.-H. Lee, P.-T. Chou, *J. Am. Chem. Soc.* **2007**, *129*, 4534–4535.

[16] M. J. S. Dewar, E. G. Zoebisch, E. F. Healy, J. J. P. Stewart, *J. Am. Chem. Soc.* **1985**, *107*, 3902–3909.

[17] a) J. E. Ridley, M. C. Zerner, *Theor. Chim. Acta* **1973**, *32*, 111–134; b) J. E. Ridley, M. C. Zerner, *Theor. Chim. Acta* **1976**, *42*, 223–236; c) A. D. Bacon, M. C. Zerner, *Theor. Chim. Acta* **1979**, *53*, 21–54.

[18] a) M. Adachi, Y. Murata, S. Nakamura, *J. Org. Chem.* **1993**, *58*, 5238–5244; b) W. M. F. Fabian, S. Schuppler, O. S. Wolfbeis, *J. Chem. Soc. Perkin Trans. 2* **1996**, 853–856.

[19] C. A. Heller, R. A. Henry, B. A. Mclaughlin, D. E. Bills, *J. Chem. Eng. Data* **1974**, *19*, 214–219.

[20] *teXsan: Crystal Structure Analysis Package*, Molecular Structure Corporation, **1985** and **1992**.

[21] A. Altomare, M. C. Burla, M. Camalli, M. Cascarano, C. Giacovazzo, A. Guagliardi, G. Polidori, *J. Appl. Crystallogr.* **1994**, *27*, 435.

[22] P. T. Beurskens, G. Admiraal, G. Beurskens, W. P. Bosman, R. de Gelder, R. Israel, J. M. M. Smits, *The DIRIF94 Program System*, Technical Report of the Crystallography Laboratory, University of Nijmegen, The Netherlands, **1994**.

Received: February 26, 2008
Published Online: April 29, 2008

